Measurement 187 (2022) 110225

Contents lists available at ScienceDirect

Measurement

journal homepage: www.elsevier.com/locate/measurement

Accuracy of refractive index spectroscopy by broadband interferometry

Yago Arosa, Carlos Damián Rodríguez-Fernández, Alejandro Doval, Elena López Lago, Raúl de la Fuente *

Nanomateriais, Fotónica e Materia Branda, Departamento de Física Aplicada, Universidade de Santiago de Compostela, Spain

ARTICLE INFO

Keywords:
Dispersion
Spectroscopy
Spectral interferometry
Uncertainty

ABSTRACT

Uncertainties of refractive and group index in dispersion measurement by spectrally resolved white light interferometry are deeply analyzed. First, the contribution to uncertainty of the different parameters affecting both indices is identified. Afterwards, results are presented for a 1.5 mm thick fused silica sample over a broad spectral range, from 400 to 1000 nm, and the effects that mostly deteriorate the measurement accuracy are established. Finally, the different contributions are quadratically combined to determine the total uncertainty of the two indices.

1. Introduction

The possibility of using spectrally resolved white light interferometry (SRWLI) as a refractometric technique was already suggested in the early 1990s [1]. The first studies [2,3], focused on the measurement of the refractive index and its dispersion curve, $n(\lambda)$, in a relatively wide spectral range (tens of nanometers). Soon after, these works were extended to incorporate the measurement of other dispersion parameters, mainly chromatic dispersion, $dn/d\lambda$, and group index, $d(\sigma n)/d\sigma$, where $\sigma = 1/\lambda$ is the wavenumber, although some authors evaluated higher order dispersion parameters [4,5]. All these studies aim to measure the refractive index or some kind of spectral derivative by combining spectroscopy with interferometry, and we will refer to these techniques as Refractive Index Spectroscopy by Broadband Interferometry (RISBI). Like other techniques based on SRWLI, to apply RISBI we basically need three elements: a broadband source, an interferometer, and a spectrometer. RISBI was used to measure the dispersion of reference materials, both isotropic [6–10] and anisotropic [11–13], to measure dispersion in fibers [14–17], to determine the group delay of dispersive mirrors [18,19], to measure ocular dispersion [20], to calculate thermo-optical coefficients [21], visualization of thermal lens effect [22] or to model the dispersion of families of fluids [23,24]. Furthermore, while the first works applied RISBI in the visible range, dispersion results in the near infrared [25,26] or even the UV range [27] can be found in the literature.

Of course, the validity of the obtained results was analyzed in many works, but the analysis was often based on comparison with the values obtained using other methods. However, in some works, [1,26,28], the precision or the uncertainty of the measurements was alluded to, but always in a simplified way, and only regarding to refractive index. In this work, we aim to evaluate the accuracy of RISBI techniques to measure the refractive and group index dispersion of a generic sample in a broad and rigorous way. To perform the study, we derived the theoretical expressions describing the contribution to uncertainty of each parameter involved in a generic RISBI measurement. The previous expressions are used, without any loss of generality, to evaluate the uncertainty of a real measurement taken with our experimental RISBI system on a fused silica sample. Note that the parameters governing the uncertainty in our device are similar to those governing uncertainty in any other RISBI device and, in consequence, our uncertainty evaluation can be easily extrapolated to other experimental setups and to the measurement of other kind of samples.

The rest of this contribution is organized as follows: in the next section, the different parameters that affect the measurements are identified and the fundamental formulas to calculate the two indices and their corresponding uncertainties are presented. In Section 3, the uncertainties associated to each of these parameters are modeled and evaluated separately, and, in Section 4, the results obtained with a thin sample of fused silica are presented and discussed. The discussion is first devoted to each parameter, and, afterwards, to their combination, which yields the final uncertainties of the indices. Finally, in Section 5, the conclusions are presented.

* Corresponding author.
E-mail address: raul.delafuente@usc.es (R. de la Fuente).

https://doi.org/10.1016/j.measurement.2021.110225
Received 13 July 2021; Received in revised form 7 September 2021; Accepted 22 September 2021
Available online 6 October 2021

2. Foundations

In a SRWLI experiment (see Fig. 1), two broadband beams are superimposed, and the interference pattern is resolved in the spectral domain. At an arbitrary wavelength, λ, the irradiance can be written as:

$$I(\lambda) = I_0(\lambda)[1 + V(\lambda)cos\varphi(\lambda)], \tag{1}$$

with I_0 the background irradiance, V the fringe visibility, and φ, the phase difference between the light beams. In the case in which one of the beams passes through a transparent plate of thickness d, the phase difference is given by:

$$\varphi(\lambda) = \frac{2\pi}{\lambda}[d(n - n_A) - n_A l], \tag{2}$$

where n and n_A are the plate and air refractive index, respectively, at wavelength λ, and l is the path difference travelled by one of the beams with respect to the other, in air. In this expression, it is assumed that no path difference has been introduced other than that generated in the thin plate and in air propagation. It is important to stress that the computed phase differs from that given by the equation by a multiple of 2π. This is because the arc cosine is a multivalued function or, in other words, different phases differing by a multiple of 2π result in the same value of the cosine. Therefore, when calculating the refractive index, we have an ambiguity that results from this lack of definition of the phase. Specifically, the refractive index at a wavelength λ is calculated as

$$n = n_A + \frac{1}{d}\left(\frac{\lambda\varphi}{2\pi} + n_A l + k\lambda\right), \tag{3}$$

where k is an unknown integer. Using this equation and the well-known formula for the propagation of uncertainties, we obtain the uncertainty of the refractive index, Δn as[1]:

$$\Delta n = \frac{1}{d}\sqrt{\left(\frac{\lambda}{2\pi}\Delta\varphi\right)^2 + (\lambda\Delta k)^2 + \left(\frac{n - n_{geq}}{\lambda}d\Delta\lambda\right)^2 + (n_A\Delta l)^2 + [(n - n_A)\Delta d]^2 + [(d + l)\Delta n_A]^2}. \tag{4}$$

In addition, in the third and fifth summands we have introduced n to abbreviate the formula and n_{geq} is the group index at the so-called equalization wavelength, that at which the irradiance has a stationary point [4,7,39], that is, the wavelength at which the phase in Eq. (2) presents a minimum and, therefore, its derivative is zero Applying this last condition it is obtained:

$$l = d\left[\frac{n_{geq}}{n_{geq}|_{air}} - 1\right] \tag{5}$$

As discussed in the introduction, in addition to refractive index, another parameter that can be calculated with RISBI is the group index, n_g:

$$n_g = \frac{d}{d\sigma}(n\sigma) = n + \sigma\frac{dn}{d\sigma}, \tag{6}$$

With σ = 1/λ, the wavenumber. Like refractive index dispersion, the group dispersion, that is, the wavelength dependence of the group refractive index, belongs to one of the fundamental dispersion characteristics of transparent optical materials. Nonlinear and ultrafast optics, optical fibers and waveguide photonics are specific areas in which group dispersion is of wide interest. From Eqs. (2) and (3), the following expression is obtained:

$$n_g = n_{gA} + \frac{1}{d}\left(n_{gA}l + \frac{1}{2\pi}\frac{d\varphi}{d\sigma}\right), \tag{7}$$

being n_{gA} the group index of air. One way to compute the phase derivative is to determine the fringe periodicity, Λ. It is [29]:

$$\Lambda(\sigma) = \frac{2\pi}{|d\varphi/d\sigma|}, \tag{8}$$

and therefore:

$$n_g = n_{gA} + \frac{1}{d}\left(n_{gA}l \pm \frac{1}{\Lambda}\right), \tag{9}$$

where the modulus and the ± sign come from the fact that the phase derivative is zero at the equalization wavelength and changes its sign at each side: negative for shorter wavelengths, and positive for longer wavelengths.

The corresponding uncertainty is, Δn_g:

$$\Delta n_g = \frac{1}{d}\sqrt{(n_{gA}\Delta l)^2 + [(n_g - n_{gA})\Delta d]^2 + \left(\frac{1}{\Lambda^2}\Delta\Lambda\right)^2}. \tag{10}$$

Eqs. (4) and (10) are the key equations of this study. To determine the value of the refractive and group index uncertainty, each term will be analyzed separately. Note that in the case of double pass interferometers, as the Michelson interferometer, one of the beams crosses the sample twice, so in the previous equations $d = 2e$, where e is the sample thickness.

3. Uncertainties

In this section, the uncertainties of the different parameters contributing to the refractive and group indices are discussed in detail. With respect to the uncertainty in the refractive index of air, an excellent review can be found in ref. [30].

3.1. Spectrometer calibration

The most common way to compute spectral irradiance is by means of a spectrometer. Here, no particular configuration will be considered, it is simply assumed that the resolution of the device is sufficient to resolve the interference fringes and that a linear camera is the spectrum sensing system. Calibration of the spectrometer consists in determining which wavelength falls in any pixel of the spectrometer camera. In a typical calibration procedure, various sources of known wavelength illuminate the camera, to establish the correspondence between pixels and wavelengths, λ(N), being N the pixel number, for the source wavelengths. Then, interpolation, polynomial fitting, or physical modeling [31–36] are used to determine a relation between wavelength and any pixel in the camera. In this work, we do this last step by means of a WLSI-based approach [37]. The process of calibration is described in detail in that reference; here, only a brief discussion is given.

Once the available sources of known wavelength allow us to identify the λ arriving at some of the pixels of the spectrometer camera, the

[1] In the third term on the root, the following approximation was performed: $(n_g/n_{geq})|_{air} \simeq 1$

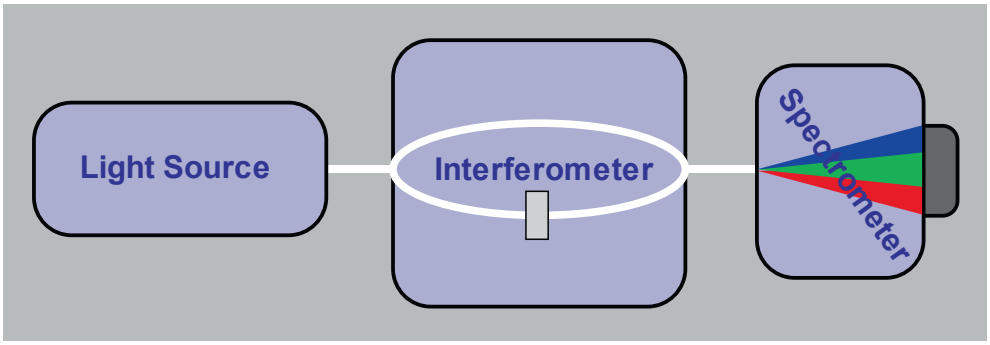

Fig. 1. Outline of a SRWLI device.

proper RISBI device without sample is used so that a broadband source illuminates the camera. By applying RISBI procedure, an array of differential phase values, φ, corresponding to every pixel is also used in order to get a set of (N,φ) points. That ϕ measurement is made for a suitable path difference, chosen to have many spectral fringes. Pairs of values of wavelength and phase difference are interesting for our purpose because if there is no sample in the interferometer, the spectral phase will be linear with the wavenumber $\sigma = 1/\lambda$ That means:

$$\varphi(N) = 2\pi l n_A \sigma(N) - 2k\pi, \tag{11}$$

where l is, as before, the path difference in air travelled by the beams. This equation can be inverted to express the wavenumber as:

$$n_A \sigma(N) = a\varphi(N) + b, \tag{12}$$

with $a = 1/(2\pi l)$ and $b = k/l$. Now, the known values of the calibration wavelengths are used to perform a linear fit and determine the constants a and b. They are employed to transform the measured phase difference into wavenumber for every pixel, providing the desired relationship $\sigma(N)$ or $\lambda(N)$. Note that this fitting can be highly enhanced by choosing a path difference l showing many resolved spectral fringes, but, obviously, the relationship $\lambda(N)$ is independent of the value of l. since different path differences corresponds to different sets of φ values. Finally, Eq. (12) furnishes the uncertainty equation:

$$\Delta\sigma = \sqrt{(a\Delta\varphi)^2 + (\varphi\Delta a)^2 + \Delta^2 b}/n_A, \tag{13}$$

together with:

$$\Delta\lambda = \Delta\sigma/\sigma^2 = \lambda^2\Delta\sigma. \tag{14}$$

To know how to evaluate Δφ in Eq. (13), see Section 3.4.

3.2. The path difference in air

The uncertainty of the path difference in air can be calculated by taking advantage of the linear relationship between phase and wavenumber in the absence of sample. Once the previous calibration was carried out, both magnitudes are related by the slope a as:

$$l = 1/(2\pi a) \Rightarrow \Delta l = l\Delta a/|a|, \tag{15}$$

where we apply the absolute value to compute the uncertainty. Although in this section we apply the same methodology as in the previous one, it is common for the path difference to be measured with a specific spectrometer of smaller spectral range than the one used to measure dispersion. This will be the case when the latter spectrometer cannot resolve the fringes associated with the measurement of l (smaller than the sample thickness, but of the same order of magnitude).

3.3. The sample thickness

If the sample is solid, its thickness can be measured directly with a high-resolution gauge. We must take into account the instrument resolution, δd_r, the flatness, δd_f, and parallelism, δd_p, of the sample surfaces. The corresponding uncertainties are $\Delta d_r = \delta d_r/\sqrt{3}$, $\Delta d_f = \delta d_f/\sqrt{3}$, and $\Delta d_p = \delta d_p/\sqrt{3}$, respectively. In addition to these uncertainties, we must include the statistical uncertainty that results from carrying out the same measurement several times.

The uncertainty estimation of liquid samples is a little more complicated since they must be introduced into a transparent cell to be measured. You can proceed in two ways: (a) measuring the total thickness of the cell, the thickness of the walls and subtracting both magnitudes to obtain the internal thickness, d; (b) directly measuring the internal thickness by applying RISBI to a liquid of known refractive index. In this case, the phase difference added by the walls must be subtracted. Typically, in both methods, the estimated uncertainty is twice that of solid samples.

3.4. Phase computation

The calculus of the phase uncertainty is undoubtedly the most complicated step. It is determined by errors in the measurement of irradiance, but the latter also affects the background irradiance and visibility. To understand the effect of the irradiance variation on the phase, pay attention to Fig. 2. It plots the actual (I) and measured irradiance ($I + \Delta I$) as a function of phase in one cycle and a bit. The oscillations are assumed to be very fast with respect to the background and visibility variation, so that we can keep the latter constant during a cycle. The irradiance variation affects both the upper and lower envelopes of the measurement as well as the phase. On the one hand, there is (or it can be) a change in the maximum and minimum values, which is associated to changes in the envelopes. On the other hand, there is also (or at least it could be) a lateral shift at any point of the interferogram, which is associated with a change in phase. Consequently, the uncertainty of the phase depends on the uncertainty of the irradiance and its envelopes. Each contribution can be determined separately.

Let us begin with the contribution of irradiance. The assumption that

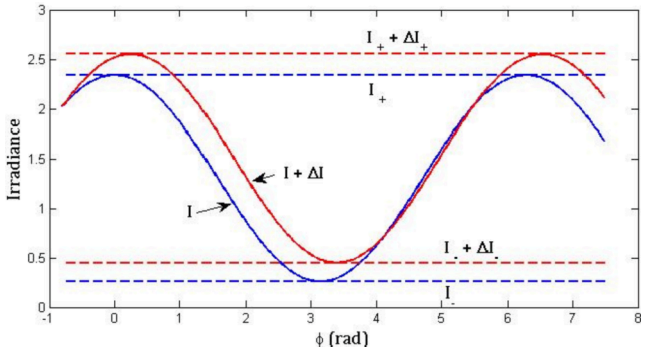

Fig. 2. Graph example of irradiance variation.

the envelopes are constant implies that the background irradiance and visibility are also constant. Therefore, from Eq. (1) it is obtained that the maximum phase variation due to irradiance is:

$$I + \Delta I = I_0[1 + Vcos(\varphi + \Delta\varphi)], \tag{16}$$

or reusing Eq. (1):

$$\Delta I = I_0 V[cos\varphi(cos\Delta\varphi - 1) - sin\varphi sin\Delta\varphi] \tag{17}$$

In addition, we can approximate $cos\Delta\varphi$ and $sin\Delta\varphi$, so that to order $\Delta\varphi^2$ we have:

$$\Delta I = -I_0 V\left[cos\varphi(\Delta\varphi)^2/2 + sin\varphi\Delta\varphi\right], \tag{18}$$

or, by reordering:

$$cos\varphi(\Delta\varphi)^2/2 + sin\varphi\Delta\varphi + \Delta I/(I_0 V) = 0. \tag{19}$$

The solutions to this equation are written as:

$$\Delta\varphi = \frac{-sin\varphi \pm \sqrt{sin^2\varphi - 2cos\varphi\Delta I/(I_0 V)}}{cos\varphi}, \tag{20}$$

where for consistency, ΔI and cosφ have opposite sign and, therefore, the solutions are real. Although both solutions are correct, only certain branches of these remain bounded and are physically valid (see Fig. 3).

On the other hand, the uncertainty is taken as positive. Therefore, the physical solution for the uncertainty can be summarized in a single equation as:

$$\Delta\varphi_0 = |tan\varphi|\left[\sqrt{1 + 2|cos\varphi|\Delta I/(I_0 V sin^2\varphi)} - 1\right], \tag{21}$$

where ΔI is assumed to be positive. This solution has two branches that meet at φ = 0 (see Fig. 3), at which:

$$\Delta\varphi_0 = \sqrt{2\Delta I/(I_0 V)}, \tag{22}$$

value which corresponds to an extreme of the solution. On the other hand, at φ =± π/2, the solutions tend asymptotically to:

$$\Delta\varphi_0 = \Delta I/(I_0 V). \tag{23}$$

Under normal conditions $\Delta I/(I_0 V) < 1$, the maximum value of uncertainty corresponds to the one given in Eq. (22), while the minimum value is the one corresponding to Eq. (23).

In a second step, we must compute the contribution of the envelopes to the phase uncertainty. The envelopes, $I_\pm$, can be put as a function of background irradiance and visibility according to the following expressions:

$$I_\pm = I_0(1 \pm V), \tag{24}$$

and therefore, the irradiance can be recast as:

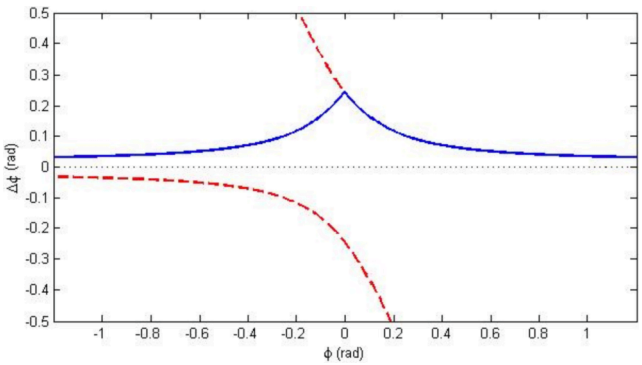

Fig. 3. Mathematical variation of the phase (dashed line) and the associated uncertainty (continuous line).

$$I = \frac{I_+}{2}(1 + cos\varphi) + \frac{I_-}{2}(1 - cos\varphi). \tag{25}$$

If we consider separately the variation of each envelope, we obtain:

$$I = \frac{I_\pm + \Delta I_\pm}{2}[1 \pm cos(\varphi + \Delta\varphi)] + \frac{I_\mp}{2}[1 \mp cos(\varphi + \Delta\varphi)] \tag{26}$$

Proceeding similarly to the previous case, and after some simple calculations, we arrive at:

$$cos\varphi(\Delta\varphi)^2/2 + sin\varphi\Delta\varphi - \Delta I_\pm(1 \pm cos\varphi)/(2I_0 V) = 0, \tag{27}$$

which is similar to Eq. (19). Therefore, solving the equation we obtain the contribution of the envelopes to the phase uncertainty:

$$\Delta\varphi_\pm = |tan\varphi|\left[\sqrt{1 + |cos\varphi|(1 \pm cos\varphi)\Delta I_\pm/(I_0 V sin^2\varphi)} - 1\right], \tag{28}$$

with $\Delta I_\pm$ positive. In particular, there is no contribution of the upper envelope to the phase uncertainty when $\varphi = (2m+1)\pi$, $m \in \mathbb{Z}$, and there is not contribution of the lower envelope when $\varphi = 2m\pi$. On the other hand, maximum uncertainty is $\Delta\varphi_\pm = \sqrt{2\Delta I_\pm/(I_0 V)}$. Putting all together and applying the law of propagation of uncertainties we obtain:

$$\Delta\varphi = \sqrt{\Delta^2\varphi_0 + \Delta^2\varphi_+ + \Delta^2\varphi_-}. \tag{29}$$

Examples of each relative contribution to the total phase uncertainty are shown in Fig. 4. As uncertainty decreases, the contribution of the irradiance approaches the sum of the contributions of the two envelopes.

3.5. Phase ambiguity

According to Eq. (3), the measured refractive index, here n_k, is a function of an arbitrary integer k for a given wavelength and sample:

$$n_k = \frac{\lambda}{d}k + a, \tag{30}$$

with a independent of k. Because of k being an arbitrary integer, the raw refractive index measured with RISBI is also arbitrary in terms of k. The variation of the refractive index produced by two consecutive values of k is:

$$\Delta n = \frac{\lambda}{d}. \tag{31}$$

That means that the error in the refractive index changes in steps of Δn. Therefore, in the case that the reference refractive index is known within a band smaller than Δn, the uncertainty associated to k can be considered null. To overcome the ambiguity, the refractive index of the sample at a fixed wavelength, λ_0, is usually measured by a second method, which provides a way to determine k. In general terms, the result of measuring the reference refractive index by whatever procedure is $n_0 \pm \delta n$, where n_0 is the measured refractive index at the wavelength λ_0 and δn its uncertainty. Hence, it can be said that the real value of the refractive index at λ_0 is contained in the interval $[n_0 - \delta n, n_0 + \delta n]$ with a high degree of confidence. This implies that we can get the correct value of k provided that:

$$\delta n \leqslant \frac{\Delta n_0}{2} = \frac{\lambda_0}{2d}, \tag{32}$$

because in this case there is only one possible value of n_k in the above interval $[n_0 - \delta n, n_0 + \delta n]$. In consequence, n_k is the value that must be taken as correct instead of the measured reference refractive index n_0. On the other hand, if Eq. (31) is not fulfilled, the value of k cannot be reliably assured. In view of this discussion, it can be said that the uncertainty in the value of k is:

$$\Delta k = \text{floor}\left(\frac{2d}{\lambda_0}\delta n\right) \tag{33}$$

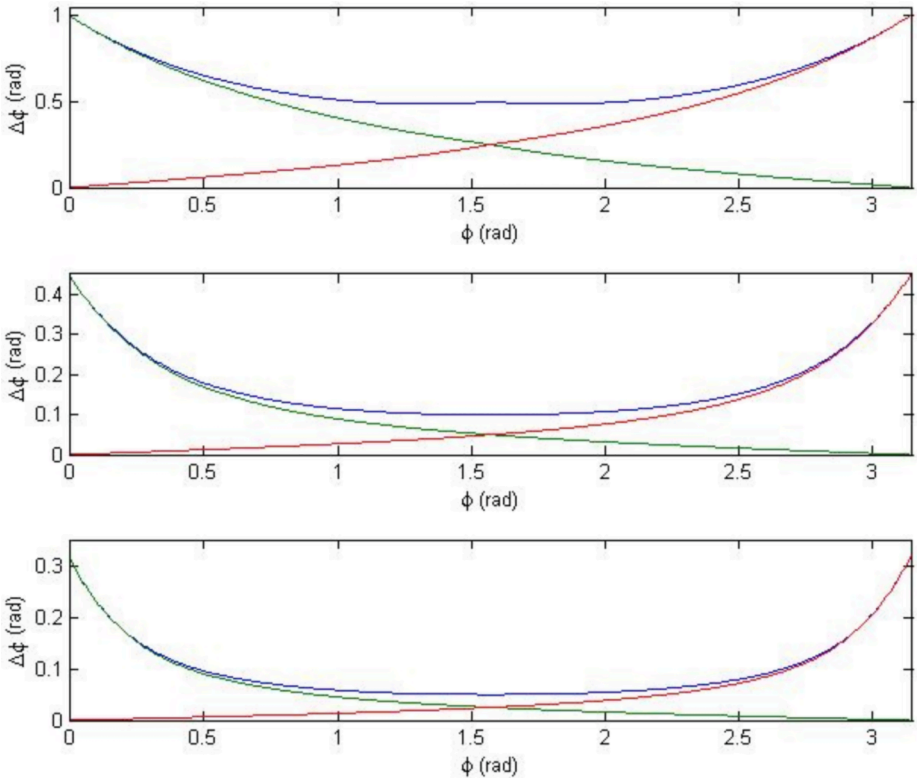

Fig. 4. Phase uncertainty related to irradiance $\Delta\varphi_0$ (blue), upper envelope $\Delta\varphi_+$ (green) and lower envelope $\Delta\varphi_-$ (red). In each case, the irradiance uncertainty is constant and equal to 5×10^{-1} (top), 1×10^{-1} (middle) and 5×10^{-2} (bottom). (For interpretation of the references to colour in this figure legend, the reader is referred to the web version of this article.)

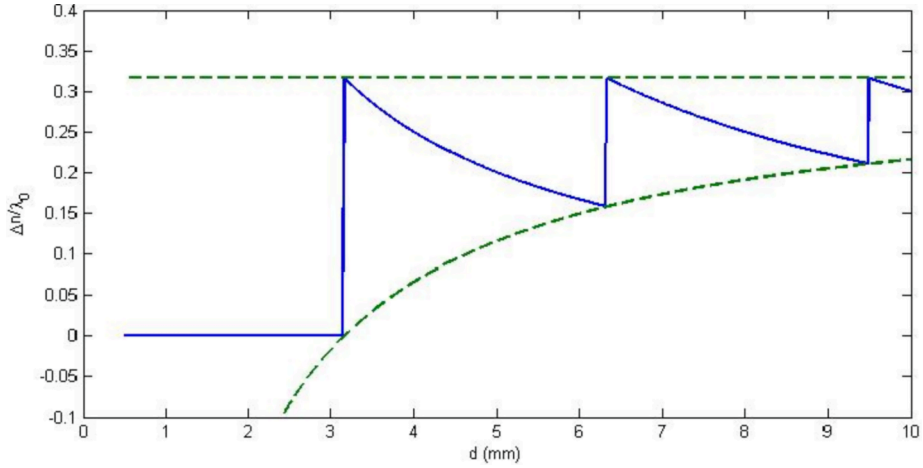

Fig. 5. Refractive index uncertainty normalized by the reference wavelength and caused by phase ambiguity against sample thickness. In this example, λ_0 = 633 nm and $\delta n = 1 \times 10^{-4}$.

Here we assume that near λ_0, $\delta n \approx \delta n_0$. So, to reduce Δk as much as possible, it is better to measure the reference refractive index at a longer wavelength. The k uncertainty contributes to refractive index uncertainty as:

$$\frac{\Delta n}{\lambda} = \frac{1}{d}\text{floor}\left(\frac{2d}{\lambda_0}\delta n\right) \tag{34}$$

In Fig. 5 this contribution is plotted for $\lambda = \lambda_0$ as a function of the sample thickness, d.

For a fixed λ, Δn makes a jump just when the argument of the floor function is an integer and, then decreases with d until another jump arises. In this figure, the upper envelope is just $2\delta n/\ \lambda_0$, and the lower envelope is $2\delta n/\ \lambda_0 - 1/d$. So, independently of the value of d, the maximum contribution to the refractive index uncertainty at wavelength λ is: $2\delta n\ \lambda/\ \lambda_0$.

3.6. Fringe spacing

The local fringe spacing, $\Lambda(\sigma)$, corresponds to the distance in wavenumber between two consecutive maxima or minima. It is also twice the distance between consecutive extremes (i.e., the absolute difference between a maximum and its adjacent minimum). So, to determine $\Lambda(\sigma)$, the extremes of the irradiance must be located. Calling $\sigma_\pm = \sigma \pm \Lambda/4$the wavenumber for two consecutive minima and

maxima, $\Lambda(\sigma)$ takes the form:

$$\Lambda(\sigma) = 2(\sigma_+ - \sigma_-), \quad \sigma = (\sigma_+ + \sigma_-)/2, \tag{34}$$

and for the uncertainty:

$$\Delta\Lambda(\sigma) = 2\sqrt{(\Delta\sigma_+)^2 + (\Delta\sigma_-)^2}. \tag{35}$$

By definition, irradiance maxima belong to the previously defined upper envelope, I_+, and irradiance minima belong to the lower envelope, I_-. As discussed above, a change in irradiance leads to a change in phase which, in turn, varies the wavenumber of the irradiance extrema. However, a change in the value of envelopes, does not affect the position of extrema but only affects to their value. So, the uncertainty in wavenumber can be written as (see Eq. 7):

$$\Delta\sigma = \frac{\Delta\varphi}{2\pi\left[dn_g - n_{gA}(d+l)\right]}, \tag{36}$$

where $\Delta\varphi$ is related to ΔI by Eq. (20). Note that once the period is determined using Eq. (34) for two extrema, it can be interpolated for any value of σ, and, for this reason, Eq. (36) applies to every σ It can also be calculated directly from the irradiance pattern by noticing that:

$$[I(\sigma_+) - I_0(\sigma_+)]/V(\sigma_+) = cos[\varphi(\sigma + \Lambda/4)] = -cos[\varphi(\sigma - \Lambda/4)] = [I_0(\sigma_-) - I(\sigma_-)]/V(\sigma_-), \tag{37}$$

and taking care that $\sigma_\pm = \sigma \pm \Lambda/4$when the uncertainty at σ is computed using Eq. (35).

4. Results and discussion

In order to evaluate the impact of the different uncertainty sources on the retrieval of refractive and group indices over a broad spectral range, we analyze in this section measurements of standard experiments carried out in our laboratory. Although results are specific to our experimental setup, the analysis is general enough to be applicable to measurements with typical RISBI devices. The main features of our RISBI system have been described elsewhere [10]. It can perform real-time dispersion measurements in a broad spectral range, from 260 to 1650 nm. With the purpose of keeping the discussion as general as possible, the results shown in this work are restricted to the interval from 400 to 1000 nm, where only one single spectrometer is used. Despite RISBI can operate with just two spectral acquisitions, one of the interferogram and another of the background irradiance, we have repeated each one of them 10 times to have statistically meaningful measurements. Indeed, it could be possible to extract the background irradiance from the interferogram, but we prefer to acquire it separately, since it allows for a double-check of the validity of the data. In Fig. 6 we show how a standard measurement with our device looks like. As it is usual in our experiments, the interferogram contains the stationary phase point, which assures good visibility in the whole spectral range, even for high dispersive samples.

To obtain information about the sample dispersion, the phase must be extracted from Eq. (1). There are a variety of methods to extract the phase from a rapid varying interferogram such as the one shown in Fig. 6. For example, applying the Hilbert, Fourier, and wavelet transforms, phase shifting methods, or phase calculation from minimum and maximum detection [39–41]. Unfortunately, many of these methods do not work well near the stationary phase point. Here, we use the procedure detailed in [10,39]. First, we separate the measured background irradiance in Eq. (1) (blue line in Fig. 6); second, we determine the upper and lower envelopes by interpolation of their maxima and minima, respectively. In this step, the stationary phase point must be omitted. The visibility function is obtained by subtraction of the two envelopes, it is removed from the equation and the cosine is extracted. Finally, the phase principal value is obtained by applying the arc cosine function.

In this section, we present results obtained with a fused silica optical window, 2 mm thick. Characteristics and manufacturer's specifications are detailed in Table 1. As in the preceding section, we analyze the impact on the measurement of each parameter separately.

Table 1
Sample parameters.

Diameter	20.0 mm
Material	UV Grade Fused Silica
Antireflection Coating	Uncoated
Surface Flatness	λ/10 @ 632.8 nm
Surface Quality	20–10 scratch-dig
Thickness	2.0 mm
Thickness Tolerance	± 0.1 mm
Wavefront Distortion	λ/10 @ 632.8 nm
Parallelism	<5 arc seconds
Clear Aperture	Central, 80% of diameter
Diameter Tolerance	+0.0/-0.2 mm

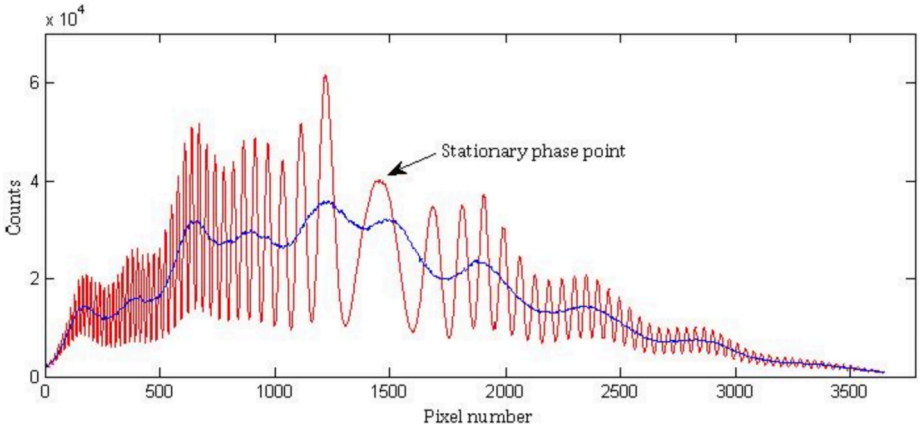

Fig. 6. Example of interferogram and background irradiance against pixel number.

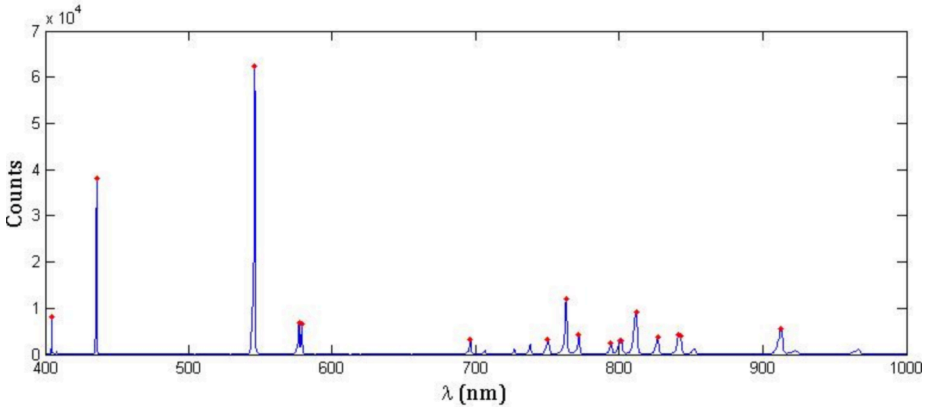

Fig. 7. Spectrum of a low-pressure Hg discharge lamp. Red points correspond to the lines used to perform the fit. (For interpretation of the references to colour in this figure legend, the reader is referred to the web version of this article.)

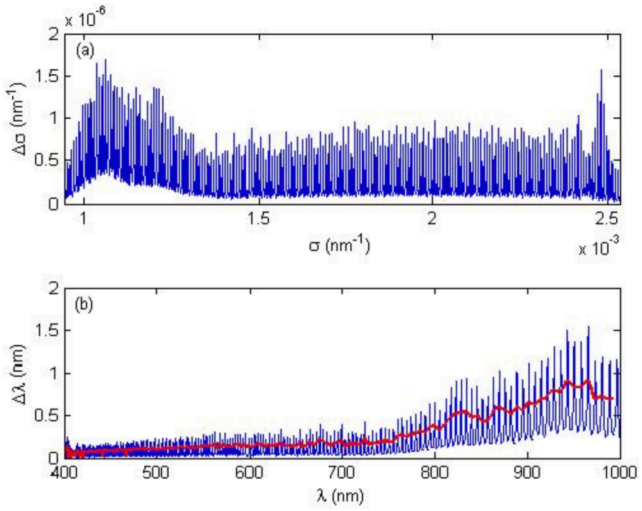

Fig. 8. (a) Wavenumber and (b) wavelength uncertainty. The red line is the local mean. (For interpretation of the references to colour in this figure legend, the reader is referred to the web version of this article.)

4.1. Spectrometer calibration

A low-pressure mercury discharge lamp was used to carry out the spectrometer spectral calibration, which is performed without sample in the interferometer. The spectra lines of this lamp in the range of measurement are shown in Fig. 7. Only the marked lines were used for calibration purposes. In order to remove any dispersion in the interferometer and ensure that induced phase difference is a linear function of the wavenumber in air, two interferograms corresponding to two different optical paths in air were taken and their phases subtracted. The computation of phase and its uncertainty was done using the method described in Section 3.4. Among the three sources of uncertainty (slope and intercept of the linear regression, and phase), the phase is the most important one. Hence, the calibration can be considered correct, but there is a need of improving the phase measurement (this will be discussed below, in Section 4.4). Fig. 8 shows that this phase uncertainty produces fast oscillations in the uncertainty of the (a) wavenumber and (b) wavelength within a period. In a real experiment, such a rapid change in uncertainty will be unrealistic and the phase is averaged over one cycle, which corresponds to the red line in Fig. 8(b).

Table 2
Sample thickness uncertainty and mean.

	Uncertainty (nm)	Mean (mm)
Resolution	58	–
Flatness	9	–
parallelism	69	–
Statistical	135	2.05713
Total	160	2.05713

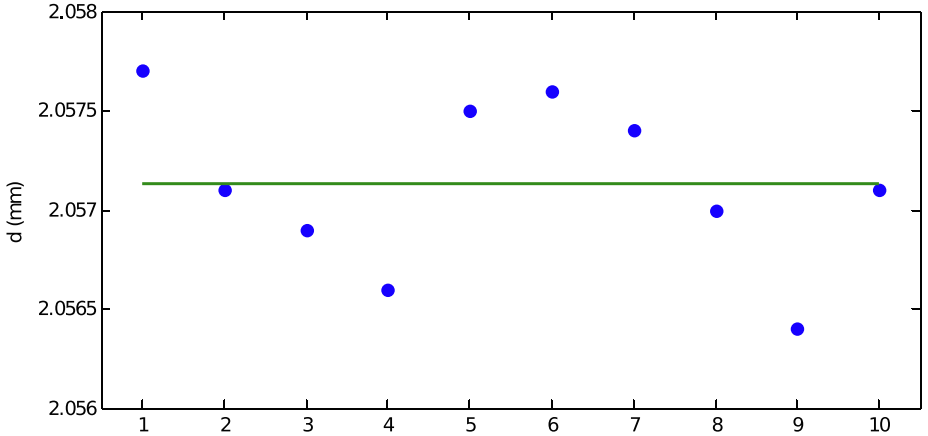

Fig. 9. Ten different measurements of the sample thickness, *d*, and their mean (green line). (For interpretation of the references to colour in this figure legend, the reader is referred to the web version of this article.)

4.2. Path difference in air

The slope of the linear regression of the calibration process can be used to extract path difference l. The uncertainty of this magnitude is straightforward to obtain, and it is $\Delta l = 141$ nm for a path difference of $l = 1.9860$ mm. Notice that these magnitudes correspond to a Michelson interferometer where light passes through the sample twice and that it will be the half in a Mach-Zehnder type interferometer.

4.3. Sample thickness

The fused silica plate thickness was measured with a high accuracy micrometer with resolution of 100 nm. The measure was repeated 10 times to get its statistical mean and its standard deviation (see Fig. 9). To calculate the uncertainty due to the sample flatness and parallelism, a beam diameter of 5 mm and centered in the sample was considered. Results are shown in Table 2. Please, note that in the case of using a Michelson interferometer, light passes through the sample twice, so both, means and uncertainties of the table, have to be multiplied by a factor of two.

4.4. Phase

There are several sources of errors that contribute to phase uncertainty. On the one hand, mechanical and thermal vibrations vary the phase in the interferometer and so the interference pattern; on the other hand, lack of visibility and noise in the spectrometer deteriorate the image interferogram. In order to take into account the different contributions, we first took up to 10 interferograms and calculated their mean plus the standard deviation, as well as the mean and standard deviation of their envelopes (in blue, in Fig. 10). Furthermore, we applied a filter in the Fourier space and quantified the difference between the filtered and unfiltered interferograms (in green, in Fig. 10) as well as the difference of the corresponding envelopes. This gives an idea of the influence of noise. As a limit, absolute values of the spectrum smaller than one thousandth of the maximum value were filtered.

Both statistical and noise contributions to the uncertainty of the irradiance are noisy, however the statistical contribution is greater in magnitude. Regarding the uncertainty of the envelopes, it is mainly constant with large modulations. While we believe that those modulations at the border of the spectrum are caused by lack of visibility, we do not recognize any possible cause of those in the center of the spectrum. However, note that they are smaller than 1% of the values of the envelope.

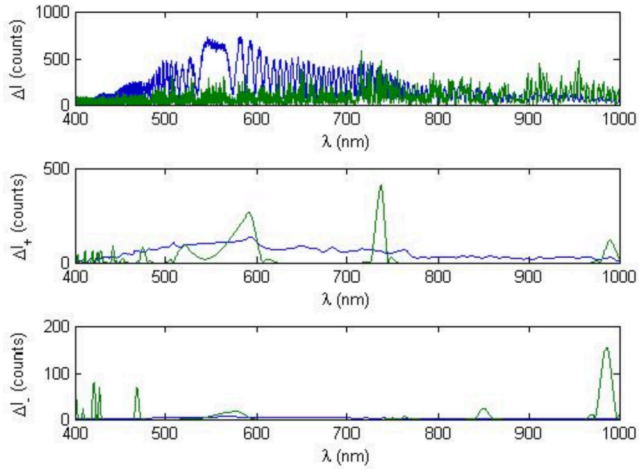

Fig. 10. Statistical (blue) and noise (green) contribution to irradiance (top), upper (medium) and lower (bottom) envelope uncertainty. (For interpretation of the references to colour in this figure legend, the reader is referred to the web version of this article.)

In Fig. 11 the three contributions to the phase uncertainty are separately shown. In agreement with the analysis in Section 3.4, all contributions present oscillations from period to period following Eqs. (21) and (28). The maxima and minima (zeros) of the phase contributions related to the upper and lower envelopes alternate at phase values multiple of π, coinciding with the maxima of the phase contribution related to the irradiance, while the minima of the later (greater than zero) occur when the phase is an odd multiple of $\pi/2$. Except at the spectrum borders, the greater contribution is related to the irradiance uncertainty, followed by the one related to the upper envelope.

In Fig. 12, which is taken as the final result of this section, the total phase uncertainty and its local average between 0.1 and 0.3 rad are shown.

4.5. Phase ambiguity

The uncertainty due to the phase ambiguity, Δk, depends on the sample thickness, the wavelength at which the reference refractive index is measured, λ_0, and the uncertainty of this measure, δn. In Fig. 13 we plot Δk against δn for our sample in both Michelson and Mach-Zehnder type interferometers, taking as reference the emission wavelength of a He-Ne laser, 632.8 nm. In the first case, there is no contribution of the phase ambiguity for δn less than 7.7×10^{-5} (the double, in the case of a Mach-Zehnder interferometer). This accuracy can be easily achieved by widely used refractometric techniques as those based on many interferometric approaches or minimum deviation methods. Indeed, commercial refractometers are available with an accuracy in the order of 5×10^{-5} or better. We note that the impact of the phase ambiguity in the refractive index uncertainty increases with sample thickness, just the opposite to the contributions of phase, thickness, and path difference in air.

In Fig. 14(a) it is shown the largest sample thickness for which the phase ambiguity contribution to the refractive index uncertainty is zero as a function of δn. In Fig. 14(b) it is plotted the contribution to the refractive index uncertainty of the minimum value of the sample thickness that produces $\Delta k = 1$, at a wavelength of 1 μm, for a varying δn too. As before, the reference wavelength is 632.8 nm.

4.6. Fringe spacing

As discussed in Section 3.6 the local periodicity is first calculated as $\Lambda(\sigma) = 2(\sigma_+ - \sigma_-)$ with $\sigma_\pm = \sigma \pm \Lambda/4$, corresponding to maxima and minima of the interferogram. That means that σ is close to a point where the irradiance equals the background ($\varphi = \pi/2$). Then, the periodicity is interpolated to cover all the measured points. The result is plotted in Fig. 15. The periodicity goes from approximately 10 nm at the spectrum borders to infinity at the equalization wavelength. Since the periodicity is proportional to the phase uncertainty, it shows oscillations as depicted in Fig. 16.

4.7. Spectrometer calibration and material dispersion

The wavenumber and wavelength uncertainties associated to the spectrometer calibration were modeled in section 3.1 (Eqs. 13 and 14) and, in section 4.1, they were quantified for the Vis-NIR spectrometer of our RISBI device (Fig. 8). The next step consists in introducing the wavelength uncertainty in Eq. (4) to compute its contribution to the total refractive index uncertainty (third term in the square root). Since the expression of the group index in Eq. (9) is independent of wavelength, it means that there is not a similar contribution to the group index uncertainty. Therefore, it could seem that the measured group index dispersion is independent of spectrometer calibration and of any miscalibration. This is meaningless. The explanation is that Eq. (10) refers only to the group index uncertainty that comes from the effect of the parameters that appear in the expression used to compute the group

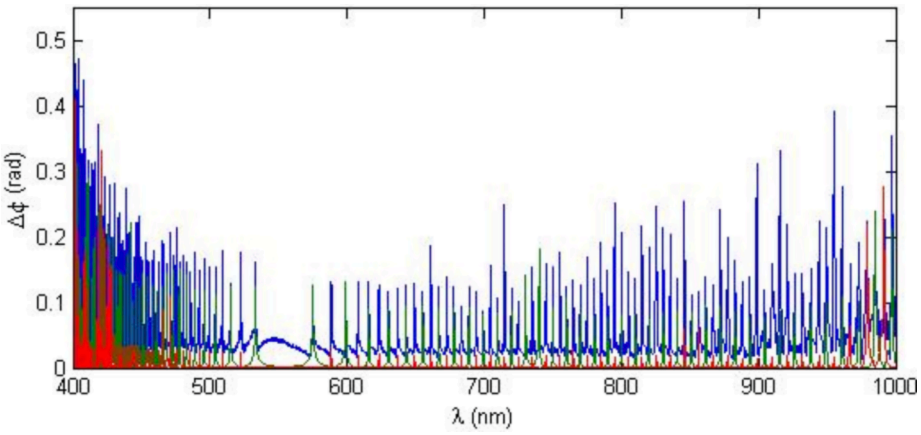

Fig. 11. Contributions to the phase uncertainty related to the irradiance (blue), upper envelope (green) and lower envelope (red). (For interpretation of the references to colour in this figure legend, the reader is referred to the web version of this article.)

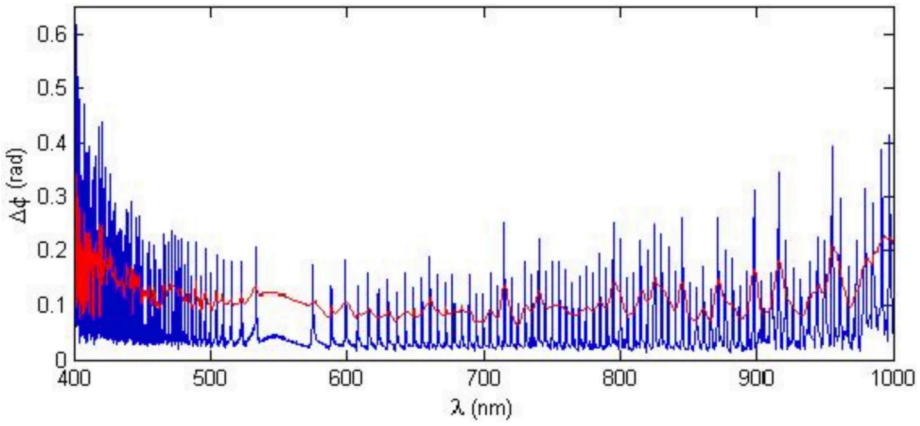

Fig. 12. Total phase uncertainty and its local average.

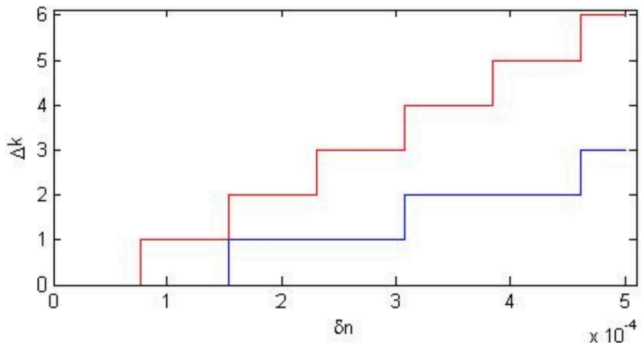

Fig. 13. Error in k as a function of uncertainty of the reference refractive index for a Mach-Zehnder (blue line) and Michelson (red line) type interferometer. (For interpretation of the references to colour in this figure legend, the reader is referred to the web version of this article.)

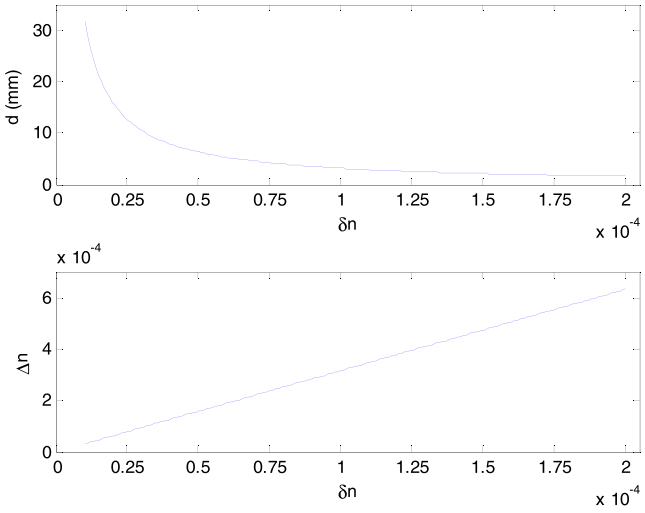

Fig 14. Largest d for which Δk is zero as a function of δn (top) and the contribution to refractive index uncertainty at a wavelength of 1 μm if $\Delta k = 1$ (bottom).

index given in Eq. (9). However, the dependence on Δλ, and thus on any calibration error, appears as soon as the dispersion curve, $n_g(\lambda)$, is considered. That is, if for a particular wavelength λ there is a miscalibration Δλ, it means that the value of the group index at this wavelength will be proportional to Δλ, and the same can be say about the refractive index uncertainty. Hence, apart from the contribution of wavelength miscalibration to the refractive index uncertainty taken into

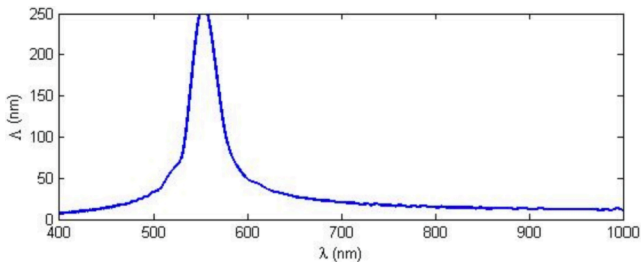

Fig. 15. Local periodicity as a function of wavelength.

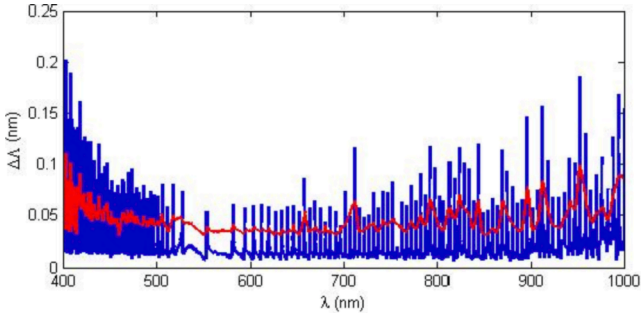

Fig. 16. Periodicity uncertainty and its local average.

account in Eq. (4), there are other "dispersive" contributions to the indices uncertainties associated to their chromatic or dispersion dependence. They can be calculated as:

$$\Delta n_D = \frac{dn}{d\lambda}\Delta\lambda$$
$$\Delta n_{gD} = \frac{dn_g}{d\lambda}\Delta\lambda, \tag{38}$$

where de subindex "D" refers to dispersion and Δλ is the wavelength uncertainty analyzed in Section 3.1. The first derivative corresponds to the chromatic dispersion, while the second one is the dispersion coefficient (usually denoted by D) multiplied by the light velocity in vacuum, c, that is, cD.

In Fig. 17 there are shown the three calibration contributions to the refractive and group index uncertainty. They are all less than 4×10^{-5} in the whole spectral range. The contribution to refractive index uncertainty included in Eq. (3) dominates the dispersion contribution except for lower wavelengths. The dispersion contribution to group index is the greater one in the first half of the spectrum while in the second part the contribution to refractive index uncertainty included in Eq. (3) dominates.

4.8. Refractive and group index uncertainty

After individually analyzing the different sources of uncertainty to refractive and group indices, all these contributions are considered together in this section. Fig. 18 shows the total refractive index uncertainty as a function of the wavelength as well as the contribution of each of the uncertainty sources. We have assumed that the phase ambiguity is well resolved so its contribution to refractive index uncertainty is zero. Below in the text, some appointments were done about this issue. In addition, the uncertainty of air refractive index is not shown since, according to [38], it is orders of magnitudes smaller than the rest of contributions ($\approx 10^{-8}$). Observing the graph, it can be concluded that the main contribution to the refractive index uncertainty results from the path difference in air, l, ($\approx 6.8 \times 10^{-5}$), followed by the sample thickness ($\approx 3.3 \times 10^{-5}$). The contribution of the calibration of the spectrometer is only relevant at IR wavelengths, whereas the phase contribution is negligeable. That gives a total refractive index uncertainty nearly constant, in the range from 7.6×10^{-5}, at visible wavelengths, to 8.3×10^{-5}, at IR wavelengths.

On the other hand, incorporating the contribution of the periodicity, the uncertainty of the group index can be computed. Fig. 19 shows the group index uncertainty together with the contributions of its different sources. In this case, the periodicity is the factor that most affects the group index uncertainty, except near the equalization wavelength, where it increases greatly. Regarding the contributions of path

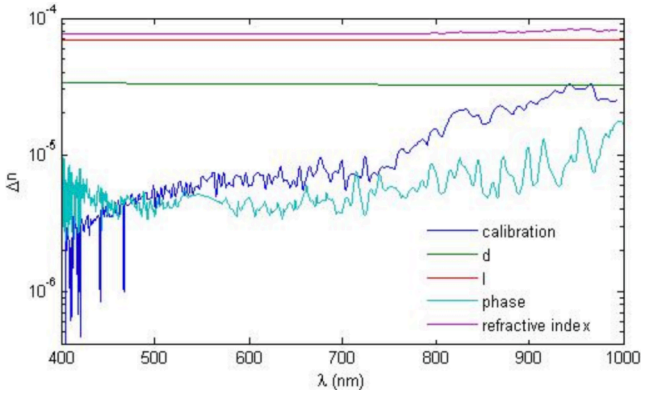

Fig. 18. The different contributions to the refractive index uncertainty and the resulting refractive index uncertainty.

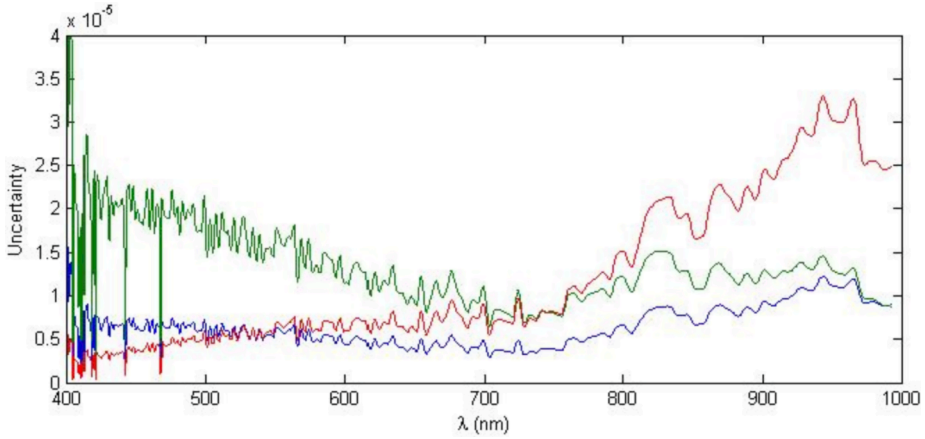

Fig. 17. The different contribution of calibration to the indices uncertainties: refractive index (blue),group index (green) dispersion and refractive index computation via Eq. (3) (green). (For interpretation of the references to colour in this figure legend, the reader is referred to the web version of this article.)

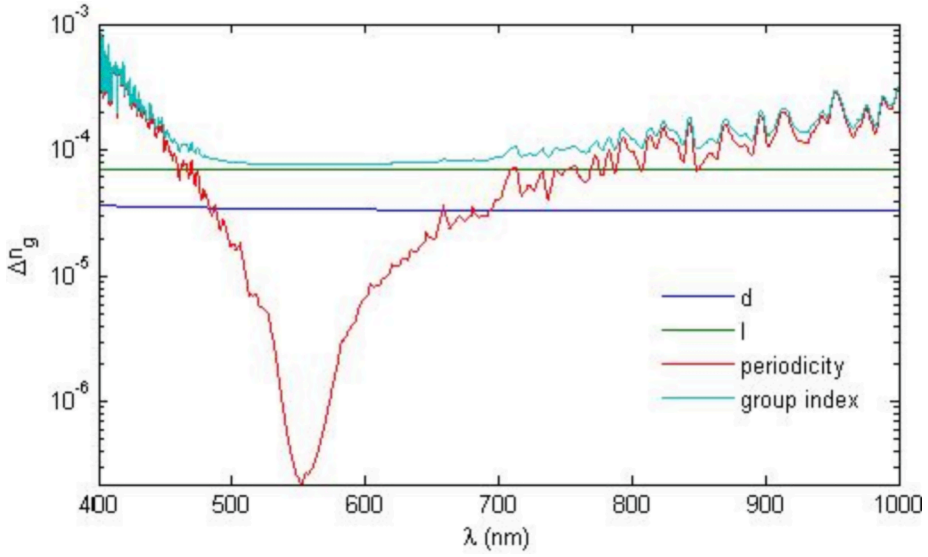

Fig. 19. The different contributions to the group index uncertainty and the resulting group index uncertainty.

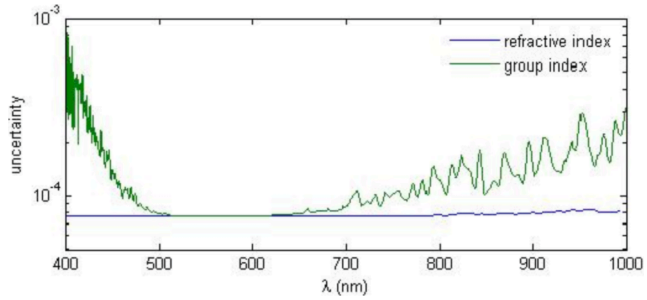

Fig. 20. Comparison between refractive and group index uncertainties.

Table 3
Uncertainty in n and n_g associated to different contributions.

	Δn (x 10^{-5})	Δn_g (x 10^{-5})
Sample thickness	3.3	3.3
Path difference in air	6.8	6.9
Calibration	< 3.5	–
Phase	< 2	–
Air index	0.001	–
Periodicity	–	< 80
Total	7.6 – 8.3	8 – 80

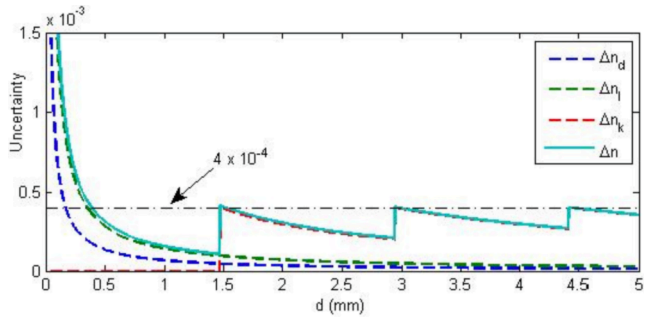

Fig. 21. Refractive index uncertainty against sample thickness. Δn_d, Δn, and Δn_k correspond to d, l and k contribution, respectively.

difference in air, l, and sample thickness, d, they are very similar to those to refractive index uncertainty, as can be appreciated comparing the expressions in Eqs. (4) and (10).

Finally, in Fig. 20, refractive and group index uncertainty are plotted together. The group index uncertainty exceeds the refractive index uncertainty in the whole spectrum, being both very similar near the equalization wavelength. At short wavelengths, the group index uncertainty reaches out values that are too high, of the order of 10^{-3}. Results are also summarized in Table 3.

4.9. The sample thickness again

We have seen that the two parameters that most effectively contribute to refractive index uncertainty are path difference in air, l, and sample thickness, d, both contributions decreasing with d. Therefore, we could think that by increasing d, the uncertainty of the refractive index could be further reduced. However, in that case, the contribution of the phase ambiguity (k) may not be negligible, and it may even exceed the previous ones if the reference refractive index is measured with not so good accuracy. In Fig. 21, we illustrate this effect by representing the total uncertainty of refractive index in addition to the contributions of d, l and k as a function of sample thickness. The considered wavelength is the Sodium D line, and the corresponding reference refractive index uncertainty is taken as 2×10^{-4}. In this case, the limiting value of the k contribution is 4×10^{-4}, and it begins to be the main contribution for sample thickness greater than 1.47 mm (0.75 if the interferometer is a Michelson one). In addition, increasing d, also produces a reduction of the fringe periodicity of the interferogram which reduces visibility, and, collaterally, increases the phase uncertainty, which becomes the most relevant contribution to group index uncertainty.

5. Conclusions

It has been proved that difference of path in air, sample thickness measurements and phase ambiguity are the factors that mostly affect the accuracy of refractive index measures in RISBI. The uncertainty related to difference of path in air and sample thickness decreases with sample thickness. In turn, phase ambiguity cancels for very thin samples but as the thickness increases it can exceed any other contribution, being limited by the measure of the reference refractive index. In the example presented, a compromise between these different components gives a smaller uncertainty for sample thickness about 1 – 1.5 mm. With respect

to the measure of group index, another parameter comes into play: the interferogram local periodicity or fringe spacing. Indeed, the measure of this parameter is the great cause of inaccuracy of group index measurement. While we have obtained refractive uncertainties less than 10^{-4}, the attained group index accuracy must certainly be improved.

We have chosen fused silica, a well-known material, to illustrate the quality and accuracy of RISBI technique but the analysis can be applied to any kind of materials, isotropic and anisotropic solids, optical fibre components or liquid sample contained in a transparent cell. For a given sample with a given material dispersion, it is a task of the researcher to select its thickness judiciously if possible, and to adapt the experimental system to obtain accurate results using RISBI.

CRediT authorship contribution statement

Yago Arosa: Methodology, Software, Formal analysis, Investigation, Visualization. **Carlos Damián Rodríguez-Fernández:** Formal analysis, Validation, Writing – original draft, Writing – review & editing. **Alejandro Doval:** Validation, Formal analysis, Investigation, Writing – original draft, Writing – review & editing. **Elena López Lago:** Validation, Project administration, Resources, Supervision. **Raúl Fuente:** Conceptualization, Methodology, Investigation, Supervision.

Declaration of Competing Interest

The authors declare that they have no known competing financial interests or personal relationships that could have appeared to influence the work reported in this paper.

Acknowledgement

The financial support of the Spanish Ministry of Economy and Competitiveness through the coordinated grants MAT2017-89239-C2-1-P is gratefully acknowledged. Moreover, this work was funded by the Xunta de Galicia and FEDER (ED431D 2017/06, ED431E2018/08, GRC 508 ED431C 2020/10).

References

[1] C. Sainz, J.E. Calatroni, G. Tribillon, Refractometry of liquid samples with spectrally resolved white light interferometry, Meas. Sci. Technol. 1 (4) (1990) 356–361.
[2] A.L. Guerrero, C. Sáinz, H. Perrin, R. Castell, J. Calatroni, Refractive index distribution measurements by means of spectrally-resolved white-light interferometry, Opt. Laser Technol. 24 (1992) 333–339.
[3] C. Sáinz, P. Jourdain, R. Escalona, J. Calatroni, Real time interferometric measurements of dispersion curves, Opt. Commun. 111 (1994) 632–641.
[4] S. Diddams, J.-C. Diels, Dispersion measurements with white-light interferometry, J. Opt. Soc. Am. B 13 (1996) 1120–1129.
[5] A.G. Van Engen, S.A. Diddams, T.S. Clement, Dispersion measurements of water with white-light interferometry, Appl. Opt. 37 (1998) 5679–5686.
[6] M. Galli, F. Marabelli, G. Guizzetti, Direct measurement of refractive-index dispersion of transparent media by white-light interferometry, Appl. Opt. 42 (2003) 3910–3914.
[7] P. Hlubina, White-light spectral interferometry with the uncompensated Michelson interferometer and the group refractive index dispersion in fused silica, Opt. Commun. 193 (2001) 1–7.
[8] R. Chlebus, P. Hlubina, D. Ciprian, Direct measurement of group dispersion of optical components using white-light spectral interferometry, Opto-Electron. Rev. 15 (2007) 144–148.
[9] D. Reolon, M. Jacquot, I. Verrier, G. Brun, C. Veillas, High resolution group refractive index measurement by broadband supercontinuum interferometry and wavelet-transform analysis, Opt. Express 14 (26) (2006) 12744, https://doi.org/10.1364/OE.14.012744.
[10] Yago Arosa, Elena López Lago, Luis Miguel Varela, and Raúl de la Fuente, "Spectrally resolved white light interferometry to measure material dispersion over a wide spectral band in a single acquisition," Opt. Express 24, 17303-17312 (2016).
[11] H. Delbarre, C. Przygodzki, M. Tassou, et al., High-precision index measurement in anisotropic crystals using white-light spectral interferometry, Appl. Phys. B 70 (2000) 45–51.
[12] G. Ghosh, Dispersion-equation coefficients for the refractive index and birefringence of calcite and quartz crystals, Opt. Commun. 163 (1999) 95–102.
[13] P. Hlubina, D. Ciprian, L. Knyblová, Direct measurement of dispersion of the group refractive indices of quartz crystal by white-light spectral interferometry, Opt. Commun. 269 (2007) 8–13.
[14] P. Hlubina, T. Martynkien, W. Urbańczyk, Dispersion of group and phase modal birefringence in elliptical-core fiber measured by white-light spectral interferometry, Opt. Express 11 (2003) 2793–2798.
[15] P. Hlubina, M. Szpulak, D. Ciprian, T. Martynkien, W. Urbanczyk, Measurement of the group dispersion of the fundamental mode of holey fiber by white-light spectral interferometry, Opt. Express 15 (18) (2007) 11073, https://doi.org/10.1364/OE.15.011073.
[16] T.M. Kardaś, C. Radzewicz, Broadband near-infrared fibers dispersion measurement using white-light spectral interferometry, Opt. Commun. 282 (2009) 4361–4365.
[17] J.Y. Lee, D.Y. Kim, Versatile chromatic dispersion measurement of a single mode fiber using spectral white light interferometry, Opt. Express 14 (24) (2006) 11608, https://doi.org/10.1364/OE.14.011608.
[18] A.P. Kovács, K. Osvay, Zs. Bor, R. Szipöcs, Group-delay measurement on laser mirrors by spectrally resolved white-light interferometry, Opt. Lett. 20, 788-790 (1995).
[19] Tatiana V. Amotchkina, Alexander V. Tikhonravov, Michael K. Trubetskov, Dirk Grupe, Alexander Apolonski, Vladimir Pervak, Measurement of group delay of dispersive mirrors with white-light interferometer, Appl. Opt. 48 (2009) 949–956.
[20] Daniel X. Hammer, Ashley J. Welch, Gary D. Noojin, Robert J. Thomas, David J. Stolarski, Benjamin A. Rockwell, Spectrally resolved white-light interferometry for measurement of ocular dispersion, J. Opt. Soc. Am. A 16 (1999) 2092–2102.
[21] A.C.P. Rocha, J.R. Silva, S.M. Lima, L.A.O. Nunes, L.H.C. Andrade, Measurements of refractive indices and thermo-optical coefficients using a white-light Michelson interferometer, Appl. Opt. 55, 6639-6643 (2016).
[22] J. Calatroni, A. Marcano, R. Escalona, P. Sandoz, Visualization and measurement of a stationary thermal lens using spectrally resolved white light interferometry, Opt. Commun. 1378 (1997) 1–5.
[23] Yago Arosa, Carlos Damián Rodríguez Fernández, Elena López Lago, Alfredo Amigo, Luis Miguel Varela, Oscar Cabeza, Raúl de la Fuente, "Refractive index measurement of imidazolium based ionic liquids in the Vis-NIR," Opt. Mater. 73, 647-657 (2017).
[24] Yago Arosa, Bilal S. Algnamat, Carlos Damián Rodríguez, Elena López Lago, Luis Miguel Varela, and Raúl de la Fuente, Modeling the Temperature-Dependent Material Dispersion of Imidazolium-Based Ionic Liquids in the VIS-NIR, J. Phys. Chem. C 122, 29470–29478 (2018).
[25] C.Z. Tan, J. Arndt, Refractive index, optical dispersion, and group velocity of infrared waves in silica glass, J. Phys. Chem. Solids 62 (6) (2001) 1087–1092.
[26] Yago Arosa, Elena López Lago, Raúl de la Fuente, "Spectrally resolved white light interferometer for measuring dispersion in the visible and near infrared range," Measurement 122, 6-13 (2018).
[27] Yago Arosa, Elena López Lago, Raúl de la Fuente, Refractive index retrieval in the UV range using white light spectral Interferometry, Opt. Mater. 82, 88-92 (2018).
[28] A. Börzsönyi, A.P. Kovács, M. Görbe, K. Osvay, Advances and limitations of phase dispersion measurement by spectrally and spatially resolved interferometry, Opt. Commun. 281 (2008) 3051–3061.
[29] Y. Arosa, R. de la Fuente, Evaluation of group index in spectrally resolved white light interferometry, Opt. Laser Technol. 133 (2021), 106507.
[30] https://emtoolbox.nist.gov/Wavelength/Documentation.asp#IndexofRefractionofAir (last access 2021-07-06).
[31] W.G. Henry, M.R. Meharry, Calibration of a prism spectrometer, J. Opt. Soc. Am. 51 (1961) 356–359.
[32] Ching-Hui Tseng, Joseph F. Ford, Charles K. Mann, Thomas J. Vickers, Wavelength calibration of a multichannel spectrometer, Appl. Spectrosc. 47 (1993) 1808–1813.
[33] Li Bai, Ningfang Liao, Zhaojian Li, Weiping Yang, Study on the wavelength calibration of type III concave grating spectrometry system, Chin. Opt. Lett. 2 (2004) 174–176.
[34] Paul Martinsen, Bob Jordan, Andrew McGlone, Paul Gaastra, Tom Laurie, Accurate and precise wavelength calibration for wide bandwidth array spectrometers, Appl Spectrosc. 62 (9) (2008) 1008–1012.
[35] Xuewei Du, Chaoyang Li, Zhe Xu, Qiuping Wang, Accurate wavelength calibration method for flat-field grating spectrometers, Appl. Spectrosc. 65 (9) (2011) 1083–1086.
[36] Kang Liu, Feihong Yu, Accurate wavelength calibration method using system parameters for grating spectrometers, Opt. Eng. 52 (1) (2013) 013603, https://doi.org/10.1117/1.OE.52.1.013603.
[37] Raúl de la Fuente, White light spectral interferometry as a spectrometer calibration tool, Appl. Spectrosc. 68 (2014) 525–530.
[38] Philip E. Ciddor, Refractive index of air: new equations for the visible and near infrared, Appl. Opt. 35, 1566-1573 (1996).
[39] Petr Hlubina, Jacek Olszewski, Phase retrieval from spectral interferograms including a stationary-phase point, Opt. Commun. 285 (24) (2012) 4733–4738.
[40] P. Hlubina, J. Luňáček, D. Ciprian, R. Chlebus, Windowed Fourier transform applied in the wavelength domain to process the spectral interference signals, Opt. Commun. 281 (9) (2008) 2349–2354.
[41] S.K. Debnath, M.P. Kothiyal, S. Kim, Evaluation of spectral phase in spectrally resolved white-light interferometry: comparative study of single-frame techniques, Opt. Laser Eng. 47 (2009) 1125–1130.